Recibido 18 Feb 2020 *ReCIBE, Año 9 No. 1, Mayo 2020*
Aceptado 21 May 2020

Industrial wireless channel measurements in a 2.4 GHz ISM radio band using a low-cost SDR-based channel sounder

Grzegorz Korzeniewski [1]
korzeniewski.gregor@gmail.com

Roberto Carrasco Álvarez[1]
r.carrasco@academicos.udg.mx

[1]CUCEI, Universidad de Guadalajara, Mexico

Abstract: Industrial wireless channel is a challenge for the design of communication systems, due to non-Line-of-Sight transmission, caused by the presence of many highly reflective obstacles, and machines in operation, which are a source of the increased noise level. The main effect, which must be analyzed, is multipath propagation. In this article, a low-cost sounding system is proposed, based on Software Defined Radio (SDR) equipment, with the intention of making sounding devices more accessible to a larger group of researchers. Likewise, the mathematical foundations and the software/hardware implementation of the wireless channel sounding system are presented, and the solutions to mitigate the synchronization issues and SDR limitations are also introduced. The performance of the proposed sounder is validated through a measurement campaign in an industrial workshop, considering the 2.4 GHz Industrial, Scientific, Medical (ISM) band. Channel sounding measurements corroborate the accuracy of the results, which converge with the channel mathematical models proposed for several industrial environments and reported in the state-of-the-art literature. In this sense, the proposed channel sounder can be used to investigate the wireless propagation environments.

Keywords: Channel sounding, Channel estimation, Industrial wireless channel, Multipath propagation, Software Defined Radio.

1 Introduction

Wireless communication is one of the greatest engineering achievements of the last several years. It has had an enormous impact on science, markets, and society, allowing us to communicate anytime, anyplace. Industry 4.0, the fourth industrial revolution, could not have come about without this technology. Its application can be found in various diagnostic and surveillance systems, sensor networks, and many others. One of the leading concepts for the modern industry is the Industrial Wireless Sensor Network (IWSN) technology, a network of sensors that can communicate with each other, increasing production efficiency throughout the industry. Another technology currently in high demand is the Internet of Things (IoT), which requires constant improvements to wireless communication systems.

Despite the abundance of improvements that wireless communication offers industry, several disadvantages must be considered. Different physical phenomena degrade the performance of a communication channel (i.e., multipath propagation, path loss, shadowing, channel interference, noise, and others), making the connection less reliable and more vulnerable. Consequently, it is important to investigate radio propagation, especially in industrial environments.

Channel sounding can be used to improve wireless communication systems. It is crucial to sound and analyze the transmission medium for network design upgrades. The knowledge obtained will increase link reliability and decrease maintenance expenses, in turn reducing production time and cost - a great benefit for industrial companies that decide to implement such innovations in their facilities.

There are various types of environments in industry, such as mines, fabrics, laboratories, etc., and each has different propagation characteristics. For example, there can be an environment which intensifies the multipath propagation effect due to many metallic objects in the area. Moreover, working electric motors in fabrics can produce shot-type noise.

To study the different propagation environments, several site-specific measurement campaigns are needed. To date, few investigations have attempted to characterize wireless channels in different industrial environments. In (Coll, 2014), channel parameters were measured in a metal workshop, a paper warehouse, a mine tunnel, and other sites. (Syed & Green, 2019) and (Düngen et al., 2019) present measurements for indoor industrial facilities with an application for IoT and industrial automation. In (Al-Samman et al., 2017), research was carried out on Ultrawideband wireless indoor channels in stationary and mobile scenarios. Similar measurements were carried out in (MacLeod et al., 2005), (Miaoudakis et al., 2005), (Luo et al., 2011). Likewise, a complete channel measurement campaign was conducted in (Cheffena, 2016) for the IWSN application. (Cheffena, 2014) presented a physical-statistical approach to channel characterization, while (Wassie et al., 2018) was focused on ultra-reliable communication techniques.

In general, the previous works were conducted using specialized and expensive channel sounding devices, such as Vector Network Analyzer (VNA), which complicates the study of new industrial propagation environments. An alternative to those systems is Software Defined Radio (SDR) based channel sounders, which are affordable and have an easily reconfigurable structure. However, there are still some serious drawbacks to this type of sounder, such as synchronization problems, sampling resolution, or hardware throughput limitations. Some projects have already implemented such SDR sounding systems (Wassie et al., 2019), (Boeglen et al., 2017), (Samayoa et al., 2018), (Hosseini & Matolak, 2018), (Maas et al., 2012) with different sounding techniques, such as OFDM modulation or the cross-correlation method. (Jamison & Frolik, 2018) has proved to be, in comparison with VNA, a highly-efficient channel sounder based on one of the cheapest SDR devices available on the market. (Boeglen et al., 2017) presented an SDR-based embedded, portable channel sounding system. (Fliedner et al., 2018) showed a design for an industrial environment channel sounder with the use of SDR equipment.

The purpose of this article is to enrich knowledge about wireless channel performance in industrial environments. A measurement campaign will be conducted in a mechanical engineering workshop, focusing on an analysis of the multipath propagation effect in the 2.4 GHz Industrial, Scientific, Medical (ISM) radio band. The collected data, together with the results from similar studies, will be helpful for network design improvements.

A further objective is to design a channel sounding system which would be accessible for a larger group of researchers, enabling the engineering society to gain a deeper comprehension of wireless propagation efficiency. The plan is to achieve this with low-cost SDR equipment. The proposed system concept and the mathematical model will be suitable for any application, environment, or frequency configuration, facilitating a possible reproduction of the presented measurement campaign in any other transmission band. Particular attention is paid for offering a solution to the synchronization problem. Additionally, system mobility will be enhanced with the use of Raspberry Pi 4 and GPS disciplined oscillators (GPSDO). Performance of the designed system will be tested by taking the aforementioned measurements in an industrial environment and validated using theoretical propagation models.

This article is organized as follows: Chapter 2 introduces the basics of radio wave propagation, while Chapter 3 presents the mathematical model of the channel sounding process. Chapter 4 explains physical implementation of the system. Chapter 5 describes the measurement campaign. Chapter 6 offers a discussion of the sounding system, and Chapter 7 presents the project conclusions.

2 Radio wave propagation concepts

In wireless communication, information is propagated by means of an electromagnetic wave. There are many phenomena that interfere with wave propagation, the most important being reflection, diffraction, and scattering. Reflection occurs when the propagated electromagnetic wave strikes an object significantly larger than the wavelength, i.e., buildings, walls, or the ground. Diffraction takes place on the sharp edges of the objects, causing the wave to bend. Scattering happens when the wave is propagated through a medium containing many small objects per unit volume (e.g. tree leaves, street signs, or lamp posts) (Rappaport, 2002).

In the following sections, the basic concepts of the radio channel and the physical phenomena that affect its performance will be explained.

2.1 Channel model

The word ”channel” can have many meanings, but in its general sense, it means everything between the signal source and its sink. Basically, a channel model can be considered a mathematical or algorithmic representation of the propagation medium’s transfer characteristics (Jeruchim et al., 2002).

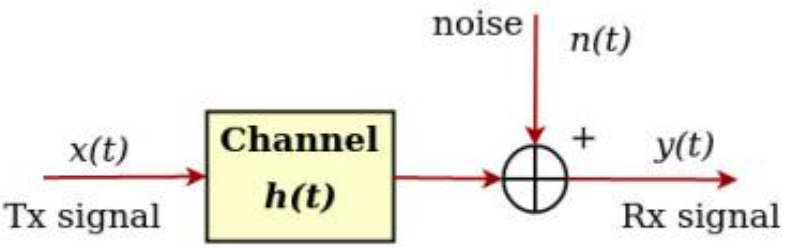

Figure 1: Basic channel model

In the figure 1, the channel model is mathematically represented as a linear, time-invariant filter with impulse response $h(t)$, whose input is the transmitted signal $x(t)$. If the signal is transmitted in the presence of white Gaussian noise $n(t)$, filtered signal and noise components are summed and the output signal $y(t)$ has the form of Equation (1) (Grzybkowski et al., 2006).

$$y(t) = \int_{-\infty}^{\infty} x(\tau)h(\tau)d\tau + n(t) \tag{1}$$

To characterize a radio channel, it is necessary to analyze the physical phenomena which assist with the propagation of electromagnetic waves and their interaction with the environment. Channel performance greatly depends on the operating frequency, the transmission environment, transceiver movement, and other factors. Typically, the channel parameter analysis is divided into two propagation modes. One of these is the Line-of-Sight (LoS) scenario, in which there are

no obstacles in the path between the transceivers (the devices ”see” each other). In the other, non-Line-of-Sight (NLoS), the path is obstructed.

Unlike the stationary and predictable wired techniques, the wireless channel is random and difficult to analyze. It is often defined as a stochastic process and requires a statistical approach for its description. In practice, many channel models are based on fitting external (empirical) observations (Stuber, 2017).

2.2 Fading channel classification

The fading channel is a communication channel which experiences variation of the attenuation of a signal as a function of time, geographic position, and radiofrequency. Fading is often described as a random process. Classification of fading types is depicted in Figure 2 (Stuber, 2017).

The two main groups of fading type are large-scale fading and small-scale fading. Large scale fading is due to distance-depended path loss of signal and shadowing provoked by large objects such as buildings and hills. Small-scale fading is characterized as rapid fluctuations of the signal over a small distance or a short period. One small-scale effect is multipath propagation, which can be further divided into flat and frequency selective fading. Small-scale fading also refers to the Doppler effect, which can be interpreted as fast or slow (Tse & Viswanath, 2004). Each of the abovementioned effects will be explained in the following chapters.

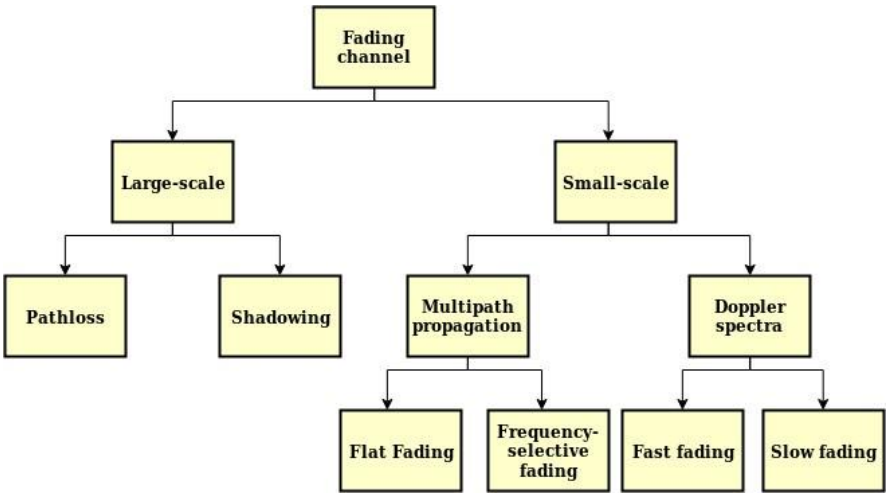

Figure 2: Fading channel classification.

2.3 Large-scale fading

Large-scale fading models signal strength over a large distance between the transmitter and the receiver. The signal received by a mobile radio from a transmitter can be represented as

$$S_r = S_t + G_{tx} + G_{rx} + L_p \qquad [dBm], \tag{2}$$

where S_r is the power of the received signal in dBm, S_t is the power of transmitted signal in dBm, G_{tx} and G_{rx} are antenna gain (dB) of a transmitter and receiver, respectively, and L_p is the propagation loss in dB. The equation 2 is often called a ”link budget”. The antenna gain depends

on the antenna's physical design, position, and orientation. The L_p component is the most difficult to define and relies on two effects: path loss and shadowing (Jeruchim et al., 2002).

2.3.1 Pathloss

Most propagation loss models are based on the fact that the average received signal power decreases logarithmically with distance. Path loss is an exponential function and can be represented by Equation 3

$$L_p = \alpha + \beta log_{10}(R) \qquad [dB], \tag{3}$$

where α and β are parameters determined by the propagation medium, and R is the transmitter-receiver separation distance. The parameter values for each model can be defined by measurement campaigns in specific environments and scenarios (Jeruchim et al., 2002).

2.3.2 Shadowing

The equation 3 does not consider the shadowing effect. In the analysis, it is necessary to include the case in which the propagated wave is "shadowed" by buildings or other obstacles, leading to the immense difference between the measured signal and its predicted average strength. It can be mathematically represented by adding to the Equation 3 a random variable X_σ, as follows

$$L_p = \alpha + \beta log_{10}(R) + X_\sigma \qquad [dB]\,. \tag{4}$$

X_σ is a zero-mean Gaussian distributed random value in dB with standard variation σ. It symbolizes a random shadowing effect that occurs over a large number of measurements for the same transmitter-receiver separation but with different obstacles in the propagation path (Rappaport, 2002).

2.4 Small-scale fading

Small-scale fading describes rapid fluctuations to signal strength over a short-range or period, so the large-scale effect can be neglected for this analysis. This fading type is the consequence of the constructive and destructive interference of the multiple signal paths between the transmitter and the receiver. This means that the radio receives many copies of the emitted signal a phenomenon known as multipath propagation. Furthermore, the movement of transceivers or enclosing objects results in the Doppler frequency shift on multipath components (Rappaport, 2002).

2.4.1 Multipath propagation

The example of multipath propagation is presented in Figure 3. Emitted waves can be reflected in the environment by reflectors, for example surrounding buildings and objects, creating "echoes" of the signal. Echoes of the signal are called multipath components. These multipath components are weighted and delayed versions of the original propagated signal, which combine at the receiver antenna. Thus, the impulse response $h(t)$ of a multipath channel is defined mathematically as follows:

$$h(t) = \sum_{m=0}^{M-1} a_m \delta(t - \tau_m), \tag{5}$$

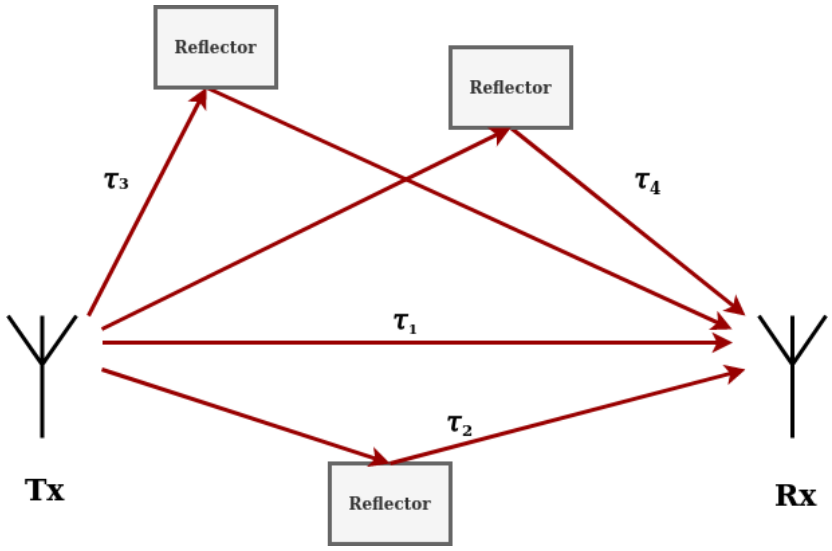

Figure 3: Example of multipath propagation.

where a_m and τ_m are the amplitude and arrival time of a m-th signal path, respectively, $\delta(t)$ is the Dirac delta function, and M is the maximum number of paths.

Each component has a random amplitude and phase, inducing small-scale signal strength fluctuations and provoking signal time dispersion and delays, leading to intersymbol interference (Rappaport, 2002). This has a significant impact on communication performance, making it crucial to analyze the following channel parameters related to this phenomenon:

- **Power Delay Profile (PDP)**, $P_h(t)$, describes the distribution of the received signal power in time from a transmitted impulse and is defined as a spatial average of squared channel impulse response $h(t)$, as follows:

$$P_h(t) = R_{hh}(0, \tau) = E\left[|h(t)|^2\right], \tag{6}$$

  where $E[\cdot]$ is the expected value and R_{hh} is the autocorrelation function.

- **Mean delay spread**, τ_{mean}, s the averaged multipath delay and is defined as the first moment of the PDP (Eq.7), with the units in seconds.

$$\tau_{mean} = \frac{\sum_i \tau_i P_h(\tau_i)}{\sum_i P_h(\tau_i)} \qquad [s] \tag{7}$$

- **RMS delay spread**, τ_{rms}, is a measurement of the channel time dispersiveness and determines the maximum symbol rate achievable by a communication system before intersymbol interference occurs. Therefore, it is often cited as the most important multipath parameter, determining the overall wireless channel performance. It is defined as the second central moment of the PDP (Eq.8) (Grzybkowski et al., 2006).

$$\tau_{rms} = \sqrt{\frac{\sum_i (\tau_i - \tau_{mean})^2 P_h(\tau_i)}{\sum_i P_h(\tau_i)}} \qquad [s] \tag{8}$$

- **Max delay spread**, τ_{max}, is the maximum time spread of the multipath components when a predefined threshold is exceeded and is defined as

$$\tau_{max} = \tau_{last} - \tau_{first} \qquad [s], \tag{9}$$

where τ_{first} and τ_{last} are the arrival time of the first and the last multipath components, respectively.
- **Coherence bandwidth**, $B_{x\%}$, is a statistical parameter that helps to define whether the channel is frequency selective over a given frequency band or frequency non-selective (flat). It is a measure of a frequency range over which the attenuation is constant and linear in phase. The coherence bandwidth has been related by inverse proportionality to τ_{rms}, as defined in the following equation:

$$B_{x\%} = \frac{1}{\alpha \tau_{rms}} \qquad [Hz], \tag{10}$$

where values of a span between 5 and 50, which corresponds to the respective correlation values of 50% and 90% (Coll, 2014).

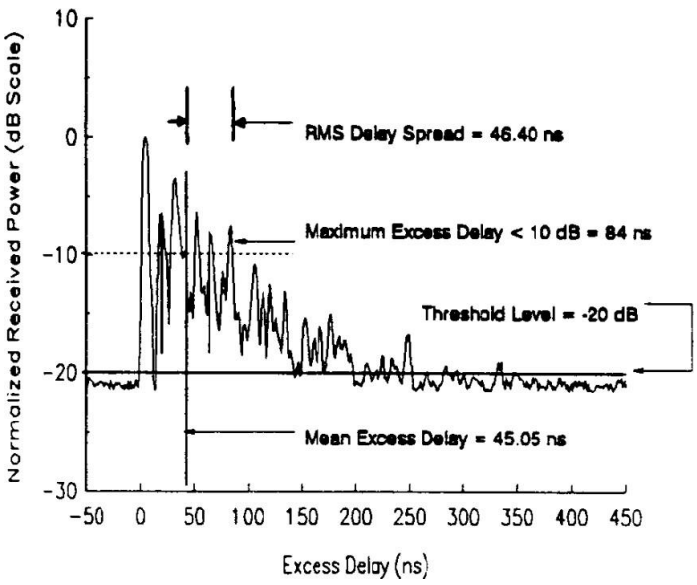

Figure 4: RMS delay spread, mean delay spread and max delay spread shown in an example of an indoor power delay profile (Rappaport, 2002).

In Figure 4, the aforementioned parameters are highlighted in the power delay profile of an indoor channel. In this example, the received power is normalized. The threshold for the maximum excess delay is set to -10 dB and the noise level to -20 dB. It can be seen that the delay values for the indoor environment are in the range of 1-200 ns.

2.4.2 Doppler Effect

The relative movement of the transmitter and the receiver cause multipath components to experience a shift in frequency. This effect is called the Doppler effect and is proportional to the velocity and motion direction of a transceiver with respect to the direction of arrival of the received multipath wave. Doppler shift f_d is given by the following equation:

$$f_d = -\frac{v}{\lambda} = -f_c\frac{v}{c} \qquad [Hz], \tag{11}$$

where f_c is the carrier frequency(in Hz), v is the velocity of the source or sink of the signal and c is the speed of light (both in $\frac{m}{s}$). Doppler shift is negative when the transceivers move away from each other (Rappaport, 2002).

2.5 Industrial environment characteristics

All the aforementioned concepts occur in the real communication system, and their intensity depends greatly on the site and surroundings. In the industrial environment, more Non-Line-of-Sight type of propagation is expected due to the communication medium being filled with obstacles, leading to signal attenuation and shadowing. Moreover, metallic machinery can provoke an intensified multipath effect caused by many reflections, diffractions, and scattering, and any random movement by people or robots in the area may cause time-variant effects in the propagation. Channel performance can be highly degraded if these phenomena are not taken into consideration when designing an industrial wireless communication system (Coll, 2014).

3 Channel sounding mathematical model

In this chapter, the mathematical foundations of the channel sounding process will be presented, showing how the channel impulse response (which is a stochastic process) can be estimated by means of cross-correlation function and white Gaussian noise. Furthermore, the estimation of PDP, using the autocorrelation matrix method, will be presented.

3.1 White Gaussian noise

The first step in designing the mathematical model is to understand what white Gaussian noise is and what its properties are. White Gaussian noise is a sequence of uncorrelated random variables with a Gaussian distribution. Without a loss of generality, an assumption of zero mean and variance $E[n^2(t)] = \sigma^2$ is made for the Gaussian noise. An important property of white noise is its constant power spectral density, meaning uniform power of each frequency. The average noise power at a period (t_1, t_2) can be calculated as follows:

$$P = E\left[\frac{1}{t_2 - t_1}\int_{t_1}^{t_2} n^2(t)dt\right] = E[n^2(t)] = \sigma^2 . \tag{12}$$

In the channel sounding process, it helps to analyze all frequencies of the bandwidth at the same time. An example of white Gaussian noise (samples in time domain and power spectral density) is shown in Figure 5.

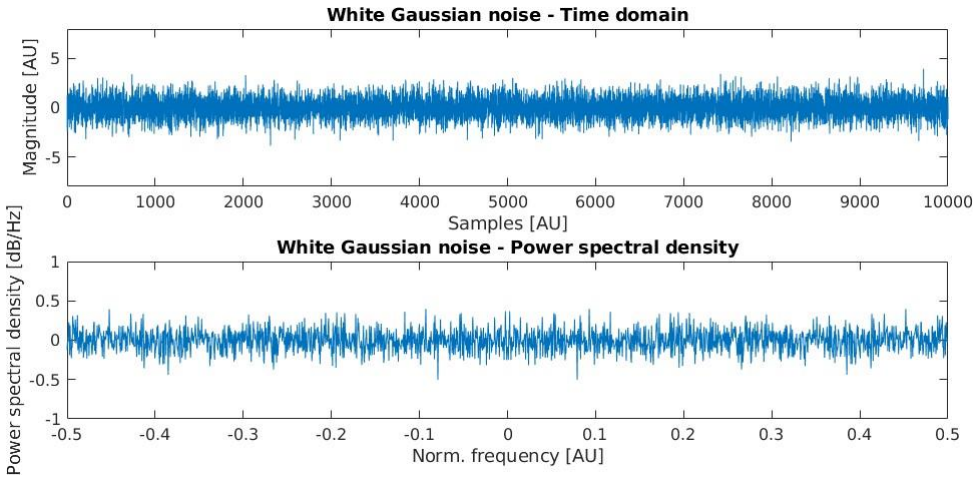

Figure 5: Example of white Gaussian noise. Time domain samples and power spectral density.

Another significant characteristic of white noise is its autocorrelation function, which is defined as:

$$R(\tau) = n(\tau) * n(-\tau) = E[n(t)n(t-\tau)] = \sigma^2\delta(\tau), \tag{13}$$

where $*$ denotes the convolution operation. This implies $R(\tau) = 0$ for any lag $\tau \neq 0$. The autocorrelation function of white noise will play a crucial role in the design of a channel sounding process (Hayes, 1996).

3.2 Channel impulse response estimation

Cross-correlation is a measure of similarity of two signals as a function of the displacement of one relative to the other. This function will be used to estimate the channel impulse response. By definition, the cross-correlation function between signal $y(t)$ and $x(t)$ can represented as (Proakis & Manolakis, 2006)

$$R_{yx}(\tau) = y(\tau) * x(-\tau)\,. \tag{14}$$

The channel can be thought of as a Linear, Time-Invariant system (LTI). The output signal $y(t)$ of the system can be represented as a convolution of the impulse response function $h(t)$ and the input signal $x(t)$ (Sharif & Sha'ameri, 2007)

$$y(t) = h(t) * x(t)\,. \tag{15}$$

In this case, the input of the system $x(t)$ will be white Gaussian noise and $h(t)$ is the channel impulse response that will be estimated.

If the signal $y(t)$ in the Eq.14 is substituted by the signal definition shown in Eq.15, the cross-correlation can be represented as follows:

$$R_{yx}(\tau) = y(\tau) * x(-\tau) = h(\tau) * x(\tau) * x(-\tau)\,. \tag{16}$$

It can be easily seen that $x(\tau) * x(-\tau)$ is the autocorrelation of white noise (eq. 13).

$$R_{yx}(\tau) = h(\tau) * x(\tau) * x(-\tau) = h(\tau) * R_{xx}(\tau) = h(\tau) * \sigma^2\delta(\tau)\,. \tag{17}$$

Using convolution properties for scalars and delta functions, the equation is developed in the following manner:

$$R_{yx}(\tau) = h(\tau) * \sigma^2\delta(\tau) = \sigma^2 h(\tau), \tag{18}$$

where σ^2 is the average power of the input signal.

As proved by means of equations 14 - 18, the cross correlation function of an output signal of a system with white noise input is equal to the system's impulse response

As noted above, the channel impulse response function is a stochastic process. To improve estimation, it is necessary to analyze several realizations of the process. Cross-correlation should be repeated several times, and the results should be averaged to obtain a better channel impulse response estimation.

3.3 Estimation of power delay profile

The next part of the channel analysis is to estimate the power delay profile. For this, the autocorrelation function will be calculated using the previously estimated channel impulse response $h(t)$, as shown in the Eq.6.

The autocorrelation function is a second-order statistical characterization of a random process. Before this function can be computed, a conversion of the continuous impulse response $h(t)$ into discrete domain $h[n]_C$ is needed, which is carried out as follows:

$$h(t) * g(t)|_{t=nT_s} = h[n], \tag{19}$$

where T_s is the sampling period, and $g(t)$ is the function that delimits the signal bandwidth to a certain value.

As a result, the discrete impulse response $h[n]$ can be represented, based on the Equation 5, as follows:

$$h[n] = \sum_{m=0}^{M-1} a_m g(nT_s - T_m), \tag{20}$$

and can be stated in a vector form as:

$$h[n] = \big[h[0], h[1], h[2] \ldots, h[p-1]\big], \tag{21}$$

where p is given by the maximum delay of a_m and the duration of $g(t)$ function.

The autocorrelation function R_{hh} of impulse response $h[n]$ is established as follows:

$$R_{hh}[n_1, n_2] = E\Big[\Big(\sum_{m=0}^{M-1} a_m g(n_1 T_s - T_m)\Big)\Big(\sum_{m'=0}^{M'-1} a_{m'} g(n_2 T_s - T_{m'})\Big)\Big]\,. \tag{22}$$

Further, a_m is a random variable, and for PDP estimation, is assumed to be uncorrelated scattered (US). The US assumption is satisfied if the phase of any multipath component is uncorrelated to another component with a different delay (Molisch, 2011). Thus, the final form of the autocorrelation function is

$$R_{hh}[n_1, n_2] = \sum_{m=0}^{M-1} \sigma_m^2 g(n_1 T_s - T_m) g(n_2 T_s - T_m), \tag{23}$$

where σ_m^2 is the power of the m-th component.

The autocorrelation function $R_{hh}[n_1, n_2]$ can be expressed in a matrix form, as follows:

$$\boldsymbol{R_{hh}} = \begin{pmatrix} R_{hh}[0,0] & R_{hh}[0,1] & R_{hh}[0,2] & \cdots & R_{hh}[0,p-1] \\ R_{hh}[1,0] & R_{hh}[1,1] & R_{hh}[1,2] & \cdots & R_{hh}[1,p-1] \\ R_{hh}[2,0] & R_{hh}[2,1] & R_{hh}[2,2] & \cdots & R_{hh}[2,p-1] \\ \vdots & \vdots & \vdots & & \vdots \\ R_{hh}[p-1,0] & R_{hh}[p-1,1] & R_{hh}[p-1,2] & \cdots & R_{hh}[p-1,p-1] \end{pmatrix}. \tag{24}$$

The elements of the main diagonal of the matrix $\boldsymbol{R_{hh}}$ are the values of the autocorrelation function that define the estimation of Power Delay Profile

$$P_h[n] = \left[R_{hh}[0,0], R_{hh}[1,1], R_{hh}[2,2], \ldots, R_{hh}[p-1,p-1]\right]. \tag{25}$$

4 Channel sounding implementation

In practice, the channel sounding process requires a device capable of sampling a radio signal at the desired frequency, with a suitable antenna gain and radiation pattern. The most important factor to consider is the synchronization between transceivers. The physical implementation of the channel sounding system will be presented in this chapter. Additionally, a sounding signal structure and a solution for the synchronization problem will be offered.

4.1 Equipment

The key equipment used for channel sounding is the bladeRF x40. This product from the Nuand company is an SDR, which means that the radio components (such as mixers, filters, modulators, etc.) can be implemented by software. The frequency range of 300 MHz to 3.8 GHz is suitable for measurements in the 2.4 GHz ISM band. The maximum bandwidth of the instrument is 28 MHz. It is capable of acquiring 12-bit IQ samples with a sample rate of up to 40 MS/s, which results in the maximum time resolution of 25 ns. To achieve such a high data rate between the bladeRF board and the controller unit, the producer implemented a USB 3.0 interface. BladeRF has an independent transmission and reception signal paths, so it can operate in a Full-Duplex mode. It also has an external clock port, crucial for solving the synchronization problem. Two bladeRF boards are used in the system: one for signal transmission and another for reception (Nuand, 2014).

The outcoming signal is amplified by an external power amplifier to reach 15 dBm of transmission power. A Crystek CRBAMP-100-6000 amplifier, with 18 dB gain and 1 dB compression point at 17 dBm, is used in this implementation. The received signal is amplified using bladeRF's onboard low noise amplifier. Both bladeRFs are connected, via an SMA connector, to omnidirectional antennas suitable for the 2.4 GHz frequency band. The gain of the antennas is 2 dBi and the length is 10.8 cm.

A pair of Leo Bodnar's Mini Precision GPSDOs provide a reference clock for the SDR devices. The instrument output is a 3.3 V CMOS signal. The output frequency can be programmed to any value between 400 Hz and 810 MHz. For the purposes of this project, the frequency is set to 38.4 MHz to meet the bladeRF specifications. The GPSDOs are connected to bladeRF's external clock port with an SMB cable. The device uses an active GPS antenna with a 3 m cable and is powered by 5V DC from a USB port (LeoBodnar, 2015).

In the proposed bladeRF system configuration, a controlling unit with a USB 3.0 interface and a minimum 2 GB RAM is required to both input the transmission signal to the SDR device and to receive data. The newest version of a single-board computer, Raspberry Pi 4 with 2 GB RAM, has been chosen to be the transmission side of the sounder due to its USB 3.0 ports, essential for correct sounder operation. For the reception part and system controlling unit, an ASUS N550J laptop with Ubuntu Linux 18.04 operating system, Intel Core i7 CPU, and 16 GB RAM was used.

4.2 Channel sounding system

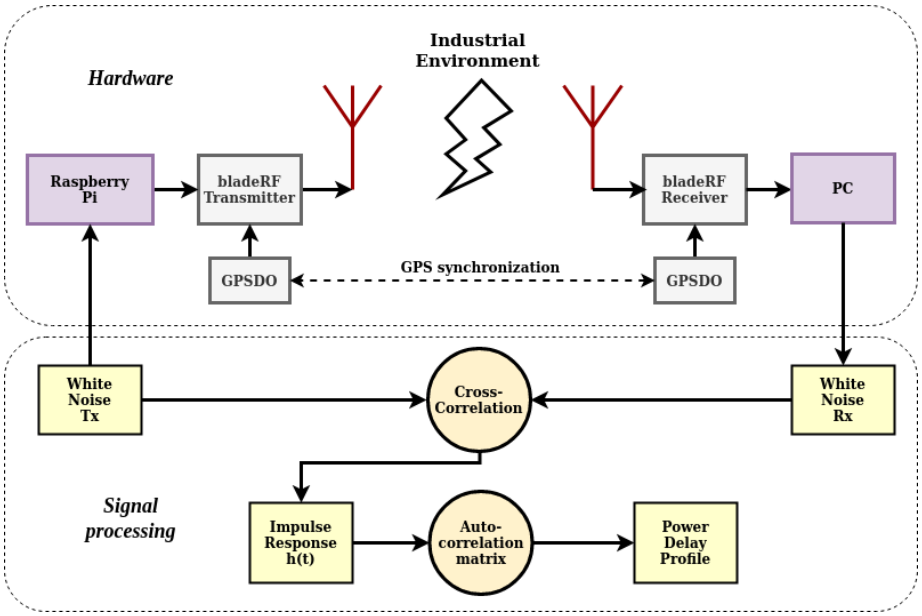

Figure 6: Sounding system diagram.

Figure 6 shows the channel sounding system, which is divided into 2 sections: hardware implementation and signal processing. The PC unit is the sounder controller unit. One of its tasks is to establish a connection (over a local WiFi network) with the remote transmission part of the system, which is controlled by Raspberry Pi, and send it a command to start the channel sounding process. The PC's other task is to handle the signal processing part of the system. Both tasks are performed by a Python program developed by the author, with the help of open-source Python libraries.

The first step of the sounding process is to generate a white noise sequence, which is produced by the PC unit and sent to Raspberry Pi. The same signal is stored for further processing in the signal processing part. The sounding signal is passed to bladeRF, amplified, and propagated through the omnidirectional antenna to the industrial environment. On the receiver side,

there is another bladeRF device connected to the antenna and controlled by the PC unit. Both bladeRF boards are controlled via USB 3.0 interface and bladeRF-cli (bladeRF Command Line Interface, a software tool provided by the board's producer) basic commands. The main problem with the sounding system is the synchronization between the transceivers, clarified in chapter 4.4. Received samples are stored and passed to the signal processing part.

The cross-correlation function of transmitted and received white noise is calculated in the signal processing section, obtaining the estimation of the channel impulse response used to compute the auto-correlation matrix in order to estimate the PDP.

The proposed system software is available in a public repository (link to the repository), which contains Python scripts and a Graphical User Interface to perform channel impulse response estimation with a user-friendly program.

4.3 Sounding signal structure

The following transmission signal structure is proposed for the sounding system: The duration of the signal is 1 second, and the signal is divided into 100 000 windows of a duration of 10 µs. Each window is filled with white Gaussian noise in a time ratio of 1% (0.1 µs), leaving the remaining part with a null value, as shown in Figure 7. This is to assure that each window will be an uncorrelated realization of the sounding process. Filling the window with only white Gaussian noise would influence the subsequent estimation, which does not coincide with the assumptions made in the mathematical model proposed in chapter 3. The estimation of the impulse response is concluded with an average of 100,000 realizations.

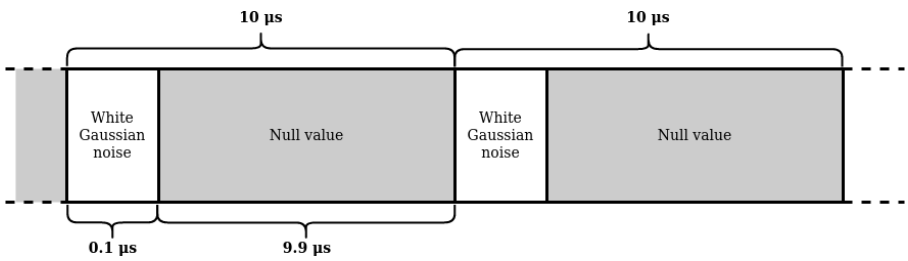

Figure 7: Sounding signal structure diagram.

4.4 Synchronization

Synchronization is an important part of the channel sounding process. Leaving this problem unsolved leads to several errors in signal modulation and processing. In SDR-based sounders, there are two issues to deal with.

The first problem to solve is radio oscillator synchronization. In the modulation process, it is crucial that the transceivers rely on the same reference clock in order to avoid synchronization errors, i.e., frequency shift. In this article, the proposed solution is to use GPSDO. This reference oscillator locks its output to pulses sent by GPS satellites. Hence, every SDR used will share the same reference clock for the modulation process.

Another synchronization process must be done in the data processing part. In order for the received white noise to correspond to the transmission sequence samples, it must first be aligned to its first sample. In practice, the sounding signal will not necessarily be at the beginning of received samples due to hardware (bladeRF and the controller unit) delays. The solution is to add

a synchronization sequence at the beginning of the transmission. In this case, a single tone of a known 20 kHz frequency is transmitted for 0.5 seconds, followed by a 0.1-second break, and then the sounding signal transmission is begun (the values were chosen empirically). A diagram of the synchronization sequence is shown in Figure 8. This enables determining precisely where the sounding process starts. It is a pure post-processing problem, meaning that this alignment is set after the transmission, not in the real-time operation.

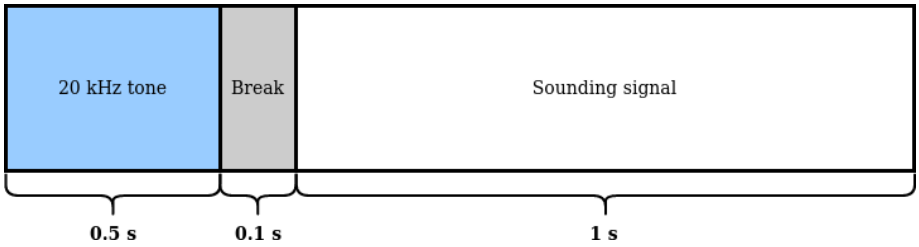

Figure 8: Transmission synchronization sequence diagram.

5 Measurement campaign results

This section describes a measurement campaign. First, the details of the measured environment will be presented. Furthermore, several data will be analyzed. The main focus of the experiment was on the multipath propagation effect. A spatially-averaged PDP was estimated and the results were compared with the Saleh-Valenzuela indoor channel model.

5.1 Environment description

The measurement campaign was performed in a workshop of the mechanic faculty at the University of Guadalajara, Mexico. The building has an open space hall with dimensions of 42 m× 18 m. It consists of concrete floor and walls, a 12-m high metallic ceiling, metallic stairs, balcony, and railings. The outside wall is made of glass. A view of the workshop is shown in Figure 9.

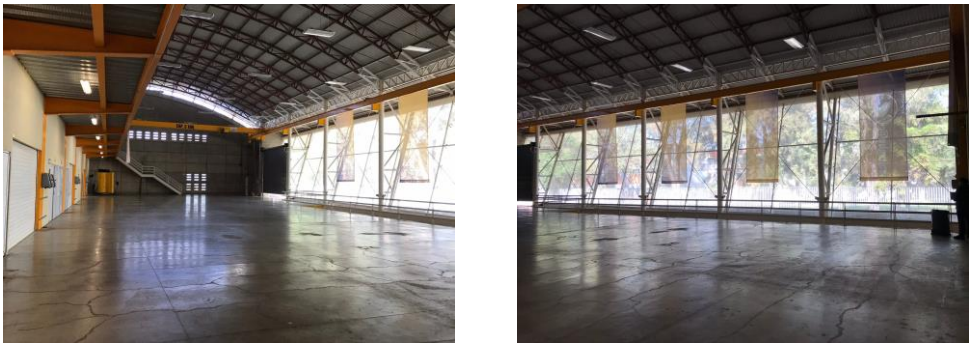

(a) (b)

Figure 9: A view of the workshop, where the experiment was performed: a) General view b) Glass wall

Due to the absence of machinery or other obstacles, each measurement was performed in a Line-of-Sight scenario. There was no movement during the experiment by the antennas, the people, or the objects.

Figure 10 presents the building dimensions along with measurements points. The transmitting antenna was situated at a fixed position Tx, and the receiver antenna at four different measurement points (Rx1-Rx4). It is worth noting that the Rx1 point was placed under the balcony. The height of the transmitter and receiver antenna was 0.45 m and 0.75 m, respectively.

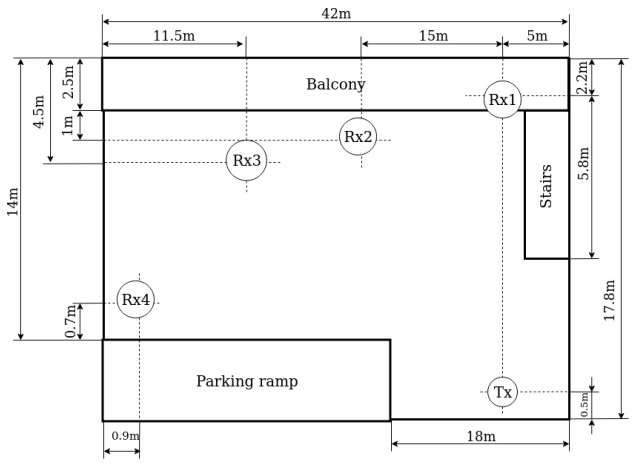

Figure 10: Building measurements and antenna positions. Tx: transmitting antenna. Rx1-Rx4: receiving antenna positions. Note: antenna Rx1 is placed under the balcony.

5.2 Multipath propagation analysis

During the measurement campaign, the multipath propagation effect was analyzed with equipment calibrated for the carrier frequency of 2.3 GHz, 28 MHz bandwidth, and 25 ns of sample time resolution. At each Rx position, the channel was sounded 5 times and an average PDP was estimated. Figures 11 a)-d) show the estimation of normalized PDP at each measuring points.

A dominant multipath component, corresponding to the Line-of-Sight signal path, is observed in each of the estimated PDPs. Moreover, several paths are noticeably delayed and attenuated with respect to the dominant component and can be related to signal reflections off the building's walls, floor, or ceiling.

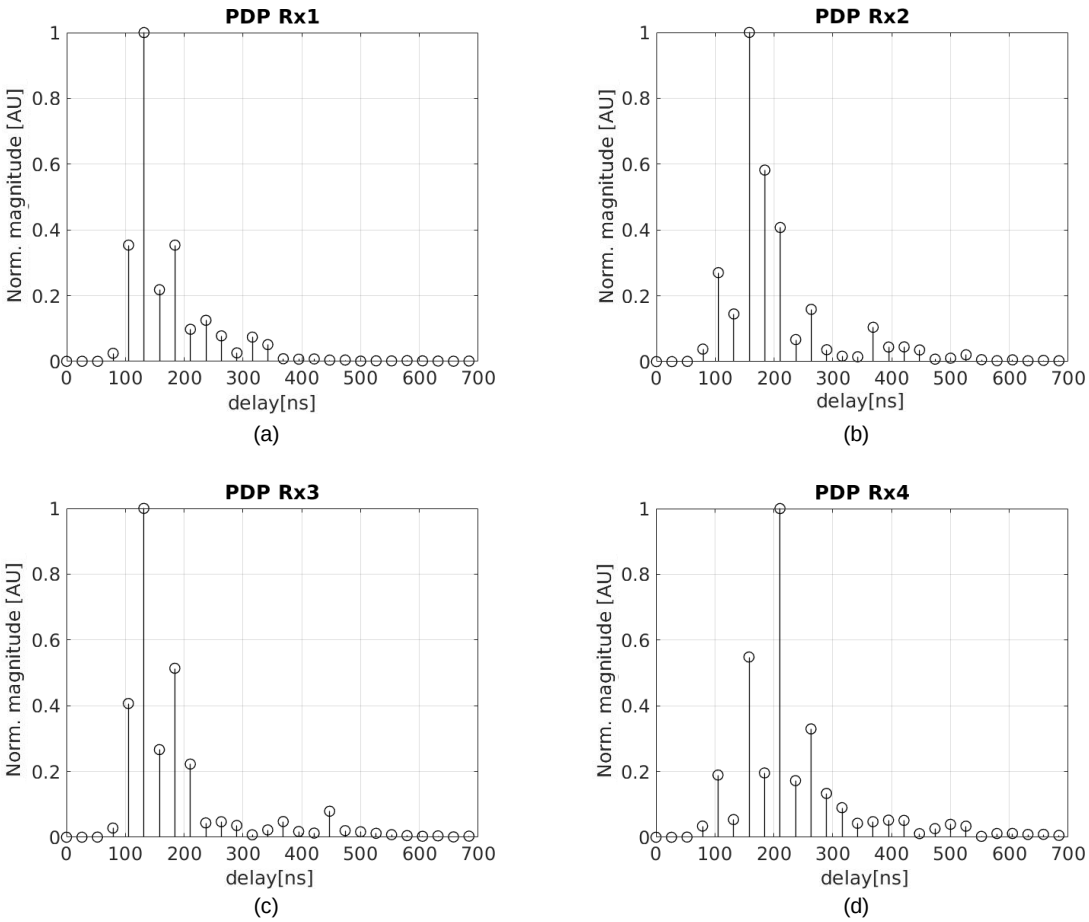

Figure 11: Estimation of normalized Power Delay Profile at measurement points: a) Rx1 b) Rx2 c) Rx3 d) Rx4.

The parameters τ_{mean} , τ_{rms} and τ_{max} were computed for each of the estimated PDPs. Furthermore, coherence bandwidth $B_{50\%}$ was estimated for the correlation value of 50%. The results are presented in Table 1, along with the separation distance.

Measurement point	Tx-Rx distance [m]	t_{mean} [ns]	t_{rms} [ns]	t_{max} [ns]	$B_{50\%}$ [MHz]
Rx1	15	162.2	57.6	263.2	3 470
Rx2	20	195.9	80.3	447.4	2 491
Rx3	28	175.5	85.5	447.4	2 340
Rx4	36	227.8	90.3	526.3	2 216

Table 1: Multipath parameters estimation

As can be seen, values of delay parameters increase with distance, while the coherence bandwidth decreases simultaneously, deteriorating wireless channel performance. Special attention must be given to t_{rms}, as it is often a crucial parameter when defining overall network link efficiency. A similar increase of distance leading to an increase of t_{rms} has been seen in the literature (Düngen et al., 2019), (Karedal et al., 2007). For the purposes of this article, an estimation model of RMS delay spread propagation, proposed in (Greenstein et al., 1997), will be used, defined as:

$$t_{rms}(d) = T_1 d^p, \tag{26}$$

where d is the distance between antennas, T_1 is the value of t_{rms} at 1m of distance, and p is the exponent of the propagation.

A curve fitting method was used to estimate the parameters of Equation 26. The estimated values are T_1 = 20.12 ns and p = 0.43. The value of the exponent p is bigger than the reported $p = 0.1$ in (Karedal et al., 2007), where an industrial hall in an NLoS scenario was analyzed on a short Tx-Rx separation (2 m to 16 m). This greater p value might be due to a different type of analyzed environment, but it also shows that in a relatively large, open space, the propagation medium tends to experience a rapid distance-related increase of t_{rms} despite its Line-of-Sight nature. Figure 12 illustrates the RMS delay spread as a function of distance between transceivers and the model approximation in logarithmic scale.

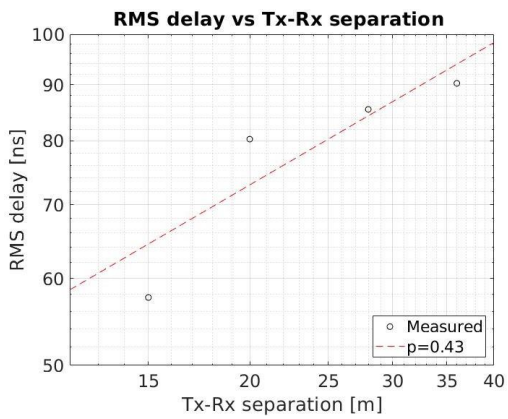

Figure 12: RMS delay spread as a function of Tx-Rx separation in logarithmic scale. Circles represent the measured data and the dashed line is the RMS delay spread propagation model with $p = 0.43$.

The next step in the analysis is to compute a spatially-averaged PDP (sPDP) using the locally estimated PDPs. sPDP is illustrated in Figure 13. Similar to the local profile outlines, a Line- of-Sight path is remarked as the dominant component, and some paths with significant delay differences are perceived as well.

The propagation parameters are estimated once again for sPDP and presented in Table 2. The measured RMS delay spread $t_{rms} = 77.2$ ns is not as high as the results for high-delay environments ($t_{rms} > 150$ ns), but greater than low-delay environment values (<30 ns), both reported in (Coll, 2014). Additionally, the estimated RMS delay is higher than a compared $t_{rms} = 34$ ns, measured for a similar environment in LoS scenario in (Syed & Green, 2019). The factors that may provoke an elevated RMS delay spread value are metallic ceiling and rails. Also, the building lacks materials that could absorb the signal energy, such as wood, paper, or others, provoking a possible RMS delay reduction. Nevertheless, the glass wall could be the element which decreases the final value of the parameter. In addition, the working area, free of metallic machinery or other obstacles in the Line-of-Sight, does not provoke an intensified signal reflection occurrence.

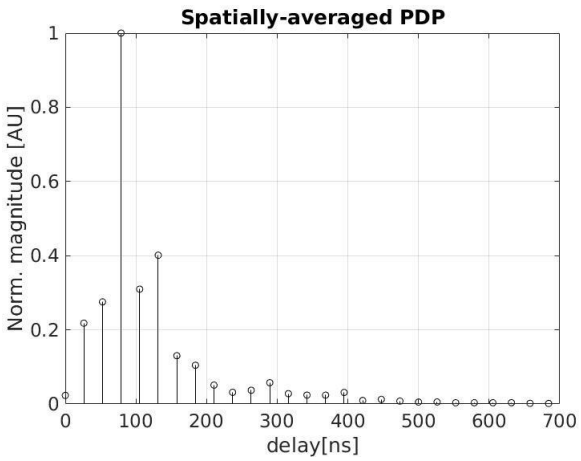

Figure 13: Spatially-averaged Power Delay Profile

Parameter	t_{mean} [ns]	t_{rms} [ns]	t_{max} [ns]	$B_{50\%}$ [MHz]
Value	113.3	77.2	447.4	2 589

Table 2: Spatially-averaged PDP multipath parameters estimation

In the following step, the measured sPDP is compared with the Saleh-Valenzuela indoor channel model (Saleh & Valenzuela, 1987) chosen because it is referenced in a wide range of studies. This simulation model separates multipath rays into groups called clusters. The power of arriving clusters decays exponentially, as do rays inside the cluster (Fig. 14).

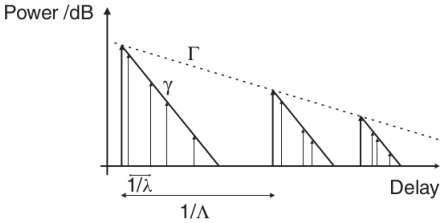

Figure 14: Saleh-Valenzuela Indoor Channel Model illustration. (Molisch, 2011)

The Saleh-Valenuzela model defines the impulse response $h(t)$ as follows:

$$h(t) = \sum_{l=0}^{L-1} \sum_{k=0}^{K-1} \beta_{kl} e^{j\theta_{kl}} \delta(t - T_l - \tau_{kl}), \tag{27}$$

where L and K are maximum number of clusters and multipath components inside clusters, respectively, β_{kl} is the amplitude of k-th ray in l-th cluster, and θ_{kl} is the phase of the kl-th ray. T_l refers to time arrival of the l-th cluster and τ_{kl} is the arrival delay of k-th ray with respect to first ray of the l-th cluster. The amplitude β_{kl} is computed with the following equation:

$$\overline{\beta_{kl}^2} = \overline{\beta^2(0,0)} e^{-T_l/\Gamma} e^{-\tau_{kl}/\gamma}, \tag{28}$$

where $\beta^2(0, 0)$ is the average power of the first ray received, Γ and γ are exponential decay constants for cluster and rays, respectively. The ray decay constant is reported to increase as a function of time delay $\gamma(\tau)$, thus is modeled as follows:

$$\gamma(\tau) = \gamma_0 + a\tau, \tag{29}$$

where γ_0 is the ray power decay constant of the first cluster and a is the function slope. The arrival times of clusters T_l and rays τ_{kl} are Poisson-distributed, with different interval time constants. Λ parameter indicates an average cluster arrival ratio (average number of clusters per nanosecond), and λ represents the same ratio for rays inside the cluster (Karedal et al., 2007).

To compute the model parameters, the sPDP samples are divided into clusters by the visual decision of the author. Decay factors are estimated with the help of the curve-fitting method. The parameters of the S-V model used for the simulation are listed in Table 3.

Parameter	Λ [1/ns]	λ [1/ns]	Γ [ns]	γ_0 [ns]	a [A.U.]
Value	0.0095	0.0358	69.2	23.65	0.062

Table 3: Used parameters of Saleh-Valenzuela model for simulation process.

Finally, the RMS delay spread of the simulated PDP is calculated and compared to the measured value, which is presented in Table 4. Figure 15 shows the comparison between the measured sPDP of the building and the simulation. As can be noted, the measured and the simulated t_{rms} value is within the same range, and the outline of model approximation PDP matches the estimated value.

Data	t_{rms} [ns]
Measured	77.2
S-V model	59.2

Table 4: Comparison of the RMS delay spread of the measured and the simulated data.

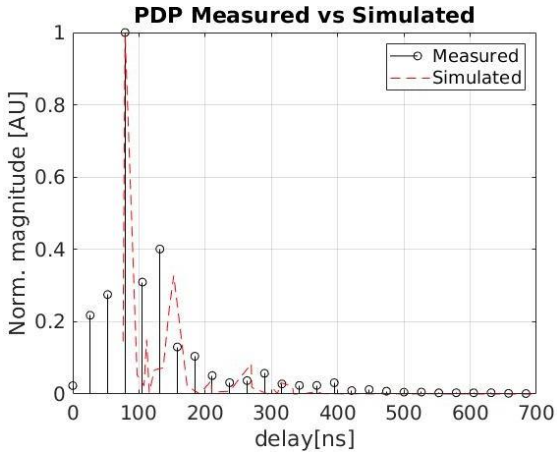

Figure 15: Saleh-Valenzuela model simulation and a comparison to the measured sPDP of the building.

6 System performance discussion

Table 5 shows a comparison of the designed system with other similar projects. The parameters compared are the software used in each project, the sampling resolution, the mobility, and the approximate system cost for a 2-node (Tx and Rx) sounder. The system cost approximation does not consider the cost of a PC unit.

Reference	Software	Samp. res.	Mobility	Approx. cost
(Maas et al., 2012)	GNU Radio	90 ns	medium	$975 USD
(Boeglen et al., 2017)	GNU Radio	25 ns	high	$12,000 USD
(Fliedner et al., 2018)	GNU Radio	10 ns	medium	$25,000 USD
(Jamison & Frolik, 2018)	GNU Radio	50 ns	high	$600 USD
(Samayoa et al., 2018)	not specified	50 ns	high	$3,000 USD
(Hosseini & Matolak, 2018)	GNU Radio	20 ns	high	$4,000 USD
(Wassie et al., 2019)	not specified	25 ns	low	$50,000 USD
Ref. VNA (Coll, 2014)	-	2 ns	low	$20,000 USD
The proposed system	Python & bladeRF-cli	25 ns	high	$1,250 USD

Table 5: Comparison of SDR-based channel sounders with the proposed system, including a VNA sounder as a reference point.

As can be seen, the achieved sampling resolution of the proposed system - 25 ns - can be considered a satisfactory value, as it is better than the values reported in (Maas et al., 2012), (Jamison & Frolik, 2018), (Samayoa et al., 2018) and equal to the sampling resolution of a more expensive high-end system presented in (Wassie et al., 2019). However, (Fliedner et al., 2018) and (Hosseini & Matolak, 2018) show that there is still room for improvement; the sampling resolution is not as high as in VNAs (<2 ns), but it is sufficient for a good multipath effect analysis.

Several factors could contribute to such a good sampling resolution. First, the use of a USB 3.0 interface between the SDR device and the controller unit eliminates ”bottlenecks” of other interfaces, i.e., the previous USB generation (USB 2.0), widely implemented in low-cost SDR devices. Second, the cross-correlation sounding method used does not require modulation techniques as other sounding routines do, which allows taking advantage of the full sampling rate provided by the SDR equipment without limiting controller unit performance. Hence, the system implementation uses only basic bladeRF-cli commands and Python libraries, which also speeds up the signal processing part. The GNU Radio, used in almost every similar project mentioned above, is a useful tool, but it consumes many controller unit processing resources and slows down the achievable system sampling rate.

Most of the aforementioned projects tend to have high sounder mobility. This is due to the nature of the small and integrated SDR boards. Additionally, mobility may be enhanced by an embedded system implementation, as presented in (Boeglen et al., 2017). The proposed sounder also follows this trend with reasonably high-mobility due to the use of Raspberry Pi 4 for the transmission part of the system. This single-board computer is a small, cheap, and powerful solution for the controlling unit.

Finally, a comparison of the approximate system costs is carried out. It can be seen that the use of SDR equipment does not necessarily mean a low-cost sounder. The budget for this project was approximately $1,250 USD, which includes two bladeRF x40 boards, two GPS DOs, a signal amplifier, and a Raspberry Pi 4 - significantly cheaper than those presented in (Wassie et al., 2019), (Boeglen et al., 2017), (Fliedner et al., 2018). The proposed sounder is within the budget range defined by those projects.

The analysis of the proposed channel sounding system performance and the comparison with similar projects will define future work. First, a change of the frequency operation range is required to perform a propagation analysis in 5.8 GHz transmission band. This will be accomplished by implementing the newer version of the bladeRF board (BladeRF 2.0) or by changing the RF front end. Second, a possible new approach to the subject would be an increased system sampling rate, as this would permit a 5G wireless channel performance analysis. It is hoped to solve this using an array of multiple synchronized SDR devices performing a shifted sampling. Another solution would be the use of an additional FPGA to act as the controller unit, replacing the limited USB interface. The authors look forward to enlarging the number of possible sounder applications by implementing MIMO propagation techniques. Lastly, a future system reconfiguration is considered to perform a real-time sounding, which could be used in cognitive radio technology to continuously sound and analyze channel performance. However, this would require a powerful processing unit, such as an FPGA or a DSP.

7 Conclusions

In this article, two achievements were demonstrated. First, the design process and the complete implementation of a channel sounding system were presented. Second, the system was used to perform a measurement campaign, whose objective was to characterize an industrial environment wireless channel.

This article offers a detailed mathematical model, a hardware implementation and a solution to the synchronization problem. The developed sounder software is available in an open repository to facilitate access to a channel sounding tool to a larger group of researchers.

The proposed wireless channel sounder system was validated with a popular Saleh-Valenzuela indoor channel simulation model and both the estimated PDP and the RMS delay spread were within the same value range, demonstrating that an SDR equipment allows a reasonable multipath effect analysis and can successfully substitute VNA devices for the sounding purpose.

The analyzed industrial environment can be identified as an intermediate delay propagation medium. The measured RMS delay spread (77.2 ns) is higher than in a high-delay environment (approx. >150 ns) and lower than in low-delay environments (approx. <30 ns). However, the estimated value is surprisingly higher than that expected for a LoS scenario. Such an increased value is due to the intensified signal reflections caused by the open hall's dimensions and building materials.

The multipath propagation effect was measured at various positions and antenna separation lengths. The collected data analysis confirms that there is an increase in the RMS delay spread as a function of distance. The delay value follows Equation 26 with parameters $T_1 = 20.12$ ns and $p = 0.43$. A comparison of the p exponent with other studies shows that this parameter is closely related to the type of environment being analyzed. Its value is influenced by building dimensions, site equipment, and machinery, and LoS/NLoS type of propagation. The analyzed workshop experienced a fast RMS delay increase.

System performance was compared to other SDR-based projects, demonstrating that the proposed system has achieved a good sampling rate (reachable for such systems) and that the proposed sounder follows the high mobility trend. In addition, the goal for a low-cost system has also been accomplished, with an approximate cost of $1,250 USD. The proposed mathematical model and solutions to SDR limitations facilitate system reconfiguration. The flexibility of this sounder encourages seeking more applications and performing more wireless channel measurements.

References

Al-Samman, A., Rahman, T., Hadri, M., Khan, I., & Chua, T. (2017). Experimental uwb indoor channel characterization in stationary and mobility scheme. *Measurement*, *111*, 333–339.

Boeglen, H., Traore, A., Peinado, M. M., Lefort, R., & Vauzelle, R. (2017). An sdr based channel sounding technique for embedded systems. In *2017 11th european conference on antennas and propagation (eucap)* (p. 3286-3290).

Cheffena, M. (2014, September). Industrial indoor multipath propagation — a physical-statistical approach. In *Ieee 25th annual international symposium on personal, indoor, and mobile radio communication (pimrc).* Washington, DC, USA.

Cheffena, M. (2016). Propagation channel characteristics of industrial wireless sensor networks. *IEEE Antennas and Propagation Magazine*, *58*(1), 66-73.

Coll, J. (2014). *Channel characterization and wireless communication performance in industrial environments* (Doctoral thesis). Department of Information Technology and Communication, KTH Royal Institute of Technology, Stockholm, Sweden.

Düngen, M., Hansen, T., Croonenbroeck, R., Kays, R., Holfeld, B., Wieruch, D., & Schulze, H. (2019). Channel measurement campaigns for wireless industrial automation. *Automatisierungstechnik*, *67*(1), 7-28.

Fliedner, N. H., Block, D., & Meier, U. (2018). A software-defined channel sounder for industrial environments with fast time variance. In *2018 15th international symposium on wireless communication systems (iswcs)* (p. 1-6).

Greenstein, L., Erceg, V., Yeh, Y., & Clark, M. (1997). A new path-gain/delay-spread propagation model for digital cellular channels. *IEEE Transactions on Vehicular Technology*, *46*(8), 477-485.

Grzybkowski, M. J., Staniec, K., & Erlebach, K. (2006). Propagation modelling. In M. Nawrocki, M. Dohler, & A. Aghvami (Eds.), *Understanding umts radio network modelling, planning and automated optimisation. theory and practice* (p. 67-115). London, England: John Wiley Sons Ltd.

Hayes, M. H. (1996). *Statistical digital signal processing and modeling*. New York, USA: John Wiley Sons Ltd.

Hosseini, N., & Matolak, D. W. (2018). Wide band channel characterization for low altitude unmanned aerial system communication using software defined radios. In *2018 integrated communications, navigation, surveillance conference (icns)* (p. 2C2-1-2C2-9).

Jamison, J., & Frolik, J. (2018). A software-defined radio approach to multi-link channel characterization. In *2018 ieee 19th wireless and microwave technology conference (wamicon)* (p. 1-4).

Jeruchim, M. C., Balaban, P., & Shanmugan, K. S. (2002). *Simulation of communication systems. modeling, methodology, and techniques* (2nd ed.). New York, USA: Kluwer Academic Publishers.

Karedal, J., Wyne, S., Almers, P., Tufvesson, F., & Molisch, A. (2007). A measurement-based statistical model for industrial ultra-wideband channels. *IEEE Transactions on Wireless Communications*, *6*(8), 3028-3037.

LeoBodnar. (2015). Mini precision gps reference clock [Computer software manual]. Northampshire, United Kingdom. Retrieved from `http://www.leobodnar.com/`

Luo, S., Polu, N., Chen, Z., & Slipp, J. (2011). Rf channel modeling of a wsn testbed for industrial environment. In *2011 ieee radio and wireless symposium* (p. 87-93). Phoenix, USA.

Maas, D., Firooz, M. H., Zhang, J., Patwari, N., & Kasera, S. K. (2012). Channel sounding for the masses: Low complexity gnu 802.11b channel impulse response estimation. *IEEE Transactions on Wireless Communications*, *11*(1), 1-8.

MacLeod, H., Loadman, C., & Chen, Z. (2005). Experimental studies of the 2.4-ghz ism wireless indoor channel. In *3rd annual communication networks and services research conference (cnsr'05).* Halifax, Canada.

Miaoudakis, G. K. A., Lekkas, A., & Koubias, S. (2005). Radio channel characterization in industrial environments and spread spectrum modem performance. In *Proc. of ieee etfa* (p. 87-93). Catania, Italy.

Molisch, A. F. (2011). *Wireless communications* (2nd ed.). London, England: John Wiley Sons Ltd.

Nuand. (2014). Bladerf x40 product brief [Computer software manual]. New York, USA. Retrieved from `https://www.nuand.com/bladeRF-brief.pdf`

Proakis, J. G., & Manolakis, D. G. (2006). *Digital signal processing* (4th ed.). Madrid, Spain: Pearson Prentice Hall.

Rappaport, T. S. (2002). *Wireless communications. principles and practice* (2nd ed.). New York, USA: Prentice Hall.

Saleh, A. A. M., & Valenzuela, R. (1987). A statistical model for indoor multipath propagation. *IEEE Transactions on Vehicular Technology*, *5*(2), 128-137.

Samayoa, Y., Kock, M., Blume, H., & Ostermann, J. (2018). Low-cost channel sounder design based on software-defined radio and ofdm. In *2018 ieee 88th vehicular technology conference (vtc-fall)* (p. 1-5).

Sharif, Z., & Sha'ameri, A. Z. (2007, December). The application of cross correlation technique for estimating impulse response and frequency response of wireless communication channel. In *The 5 student conference on research and development –scored 2007.*

Stuber, G. L. (2017). *Principles of mobile communication* (4th ed.). Atlanta, USA: Springer International Publishing.

Syed, N. A. A., & Green, P. J. (2019). Wideband communication channel sounding for wireless industrial internet-of-things applications. In *2019 ieee vts asia pacific wireless communications symposium (apwcs)* (p. 1-5).

Tse, D., & Viswanath, P. (2004). *Fundamentals of wireless communication*. Berkley, USA: Cambridge University Press.

Wassie, D. A., Rodriguez, I., Berardinelli, G., Tavares, F. M. L., Sorensen, T. B., & Mogensen, P. (2018, September). Radio propagation analysis of industrial scenarios within the context of ultra-reliable communication. In *Proc. 87th veh. technol. conf. (vtc-spring)* (p. 1-6). Porto, Portugal.

Wassie, D. A., Rodriguez, I., Berardinelli, G., Tavares, F. M. L., Sørensen, T. B., Hansen, T. L., & Mogensen, P. (2019). An agile multi-node multi-antenna wireless channel sounding system. *IEEE Access*, *7*, 17503-17516.

Esta obra está bajo una licencia de Creative Commons
Atribución-NoComercial-Compartirlgual 4.0 Internacional.